PAPER

Check for updates

Lattice engineering through Al-substitution leads to enhanced magneto-optical properties of Tb₃(AlₓGa₁₋ₓ)₅O₁₂ single crystals†

Xianhui Xin,[a] Yuankai Hao,[a] Xianxian Yang,[a] Zhen Zhang,[a] Xiuwei Fu, [ID] *[a] Zhitai Jia [ID] *[ab] and Xutang Tao [ID] [a]

High-performance magneto-optical materials are in urgent demand for high-power Faraday isolators. The traditional $Tb_3Ga_5O_{12}$ crystal presents a relatively low Verdet constant and large absorption coefficient, which makes it difficult to meet the continuous development of high-power lasers. In this work, novel $Tb_3(Al_xGa_1)_5O_{12}$ (TAGG) single crystals are grown by the Czochralski method. High-quality TAGG crystals with Al-substitution of up to 75% are obtained for the first time. The optical, thermal, and magneto-optical properties are significantly enhanced through high Al incorporation. This work demonstrates that the highly Al-substituted TAGG single crystals are remarkable magneto-optical materials for Faraday isolators.

Introduction

Magneto-optical crystals, which are capable of rotating the polarization plane of linearly polarized light,[1] are of particular interest owing to their essential applications in Faraday isolators (FIs).[2–5] There are many reported magneto-optical crystals in the

[a] State Key Laboratory of Crystal Materials, Shandong University, Jinan, Shandong 250100, China. E-mail: fxw@sdu.edu.cn, z.jia@sdu.edu.cn

[b] Shandong Research Institute of Industrial Technology, Jinan, Shandong 250100, China

† Electronic supplementary information (ESI) available. See DOI: https://doi.org/10.1039/d3tc04069k

Xiuwei Fu is currently a full professor at the Institute of Crystal Materials, Shandong University. He received his BS and MS degrees from Shandong University in 2010 and 2013, respectively, and completed his PhD degree in 2016 from Waseday University under the supervision of Prof. Kiyoshi Shimamura. Then he worked at National Institute for Materials Science (NIMS) for postdoctoral research from 2016 to 2019. His current research interest is focused on the design and growth of novel bulk single crystals for piezoelectric, magneto-optical and laser applications.

Xiuwei Fu

visible near-infrared (VIS-NIR) region so far. Among them, the $Tb_3Ga_5O_{12}$ (TGG) crystal, belonging to the rare-earth (RE) garnet family, is considered the benchmark. However, it suffers from some intrinsic drawbacks, for instance, a relatively low Verdet constant, and serious volatilization of Ga_2O_3 during growth, resulting in component deviation,[6,7] which makes high-power laser applications difficult. Over the past few decades, great efforts have been made to find magneto-optical crystals with superior Faraday effect and more favorable growth characteristics beyond TGG, including optimization of traditional magneto-optical crystals and the efficient fabrication of novel materials.

For the traditional Tb^{3+}-based TGG paramagnetic crystal, its Faraday effect originates from the $4f^8–4f^75d^1$ transition of Tb^{3+}.[8] The RE paramagnetic ions such as Dy^{3+}, Ho^{3+}, Nd^{3+} are selected as doping elements to co-occupy decahedral sites with Tb^{3+}, expecting super-exchange interaction to make TGG have a stronger Faraday effect. Although the Faraday effect of RE:TGG has been enhanced to some extent, RE paramagnetic ions have inherent absorption peaks from the VIS to NIR range. In addition, the segregation is not conducive to the growth of large-size and high-uniformity crystals, and these intrinsic drawbacks greatly affect their applications.[8–10] The $Tb_3Al_5O_{12}$ (TAG) crystal possesses excellent magneto-optical properties, but only small-size TAG single crystals have been grown by the edge-defined film-fed growth method and laser floating-zone method due to its incongruent melting nature.[11,12] In order to obtain a congruent melt, a novel magneto-optical crystal, $Tb_3Sc_2Al_3O_{12}$ (TSAG), was harvested by the replacement of Al^{3+} with Sc^{3+} in octahedral sites, but easy cracking characteristics of TSAG hinder its applications.[13] In addition, a

This journal is © The Royal Society of Chemistry 2024

J. Mater. Chem. C, 2024, **12**, 2423–2431 | **2423**

Lu-modified TSAG crystal, namely TSLAG, was also designed. Both TSAG and TLSAG preserve excellent magneto-optical performance analogous to the TAG crystal, with a Verdet constant of 25% higher than that of TGG.[7,14] Unfortunately, their practical applications are retarded due to the cation segregation and cracking problems in bulk crystal growth.

Lattice engineering is an effective strategy for property improvement. This strategy introduces modifications that change the composition and crystal field environment, further resulting in promotion in performance. Based on the quantum theory of the magneto-optical effect of the paramagnetic material, increasing the Tb^{3+} concentration per unit volume and strengthening the $4f^8$–$4f^75d^1$ transition of Tb^{3+} could lead to an enhanced magneto-optical effect for Tb^{3+}-based garnets. Both Al^{3+} and Ga^{3+} belong to the IIIA element group, and the radius of Al^{3+} is smaller than that of Ga^{3+}. Thus, compared to TGG, the replacement of Ga^{3+} with Al^{3+} to obtain $Tb_3(Al_xGa_{1-x})_5O_{12}$ (TAGG) will lead to the decrease of the lattice constant (the increase of the Tb^{3+} concentration), further bringing the enhancement of the crystal field environment. As a result, the TAGG crystal would integrate the advantages of both TGG and TAG crystals, combining the excellent properties of TAG and the good growth characteristics of TGG, while retaining the merits of the garnet structure. It has been proven to be effective since the Faraday effect and thermal properties of TAGG have been improved considerably even with a small amount of substitution.[15,16] Further increasing the Al content can lead to better magneto-optical and thermal properties. However, the relationship between Al content and properties has never been systematically studied.

Herein, in this work, the influence of Al content on the growth characteristics and properties of TAGG crystals was investigated. For this, a series of bulk TAGG single crystals were grown by the Czochralski (Cz) method. Then we presented the raw material synthesis, crystal growth, Laue back reflection patterns, high-resolution X-ray diffraction (XRD), optical, thermal, and magneto-optical properties, and composition–property relationship.

Experimental section

Crystal growth

Polycrystalline materials, including TGG, $Tb_3(Al_{0.3}Ga_{0.7})_5O_{12}$ (TAGG30), $Tb_3(Al_{0.6}Ga_{0.4})_5O_{12}$ (TAGG60), $Tb_3(Al_{0.75}Ga_{0.25})_5O_{12}$ (TAGG75) and $Tb_3(Al_{0.9}Ga_{0.1})_5O_{12}$ (TAGG90), were prepared through a traditional high-temperature solid-state method according to the following equation:

$$3Tb_4O_7 + 10xAl_2O_3 + 10(1-x)Ga_2O_3 = 4Tb_3(Al_xGa_{1-x})_5O_{12}$$
$$+ 1.5O_2. \qquad (1)$$
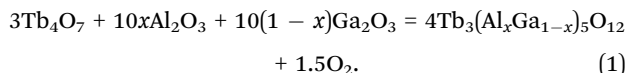
Commercial powders of 4 N purity, Tb_4O_7, Ga_2O_3, and Al_2O_3 were weighed stoichiometrically. The Ga_2O_3 raw material with a 2 wt% extra amount was added to compensate for its volatilization during the growth process. After mixing homogeneously, the powders were pressed into columns and sintered at 1450 °C

for 36 h in air to promote the solid-state reaction. All crystals were grown using the intermediate frequency Cz technique under the same growth parameters. High-purity argon was selected as a protective atmosphere during the growth process to prevent the Ir crucible from being oxidized. The $\langle 111 \rangle$ oriented TGG crystals were selected as seeds. The rotation and pulling speeds were 10–15 rpm and 1 mm h^{-1}, respectively.

Characterization

Powder XRD patterns were collected using a Bruker AXS D2 PHASER diffraction system set for Cu Kβ radiation at room temperature with a scanning speed of 0.2 s per step in an angular range (2θ) from 10° to 90°. To assess the crystalline perfection, Laue back-reflection measurements were carried out using a real-time back-reflection Laue camera system (Multiwire MWL 120 with Northstar software). The (111) oriented crystal wafers, mechanically polished on both sides, whose dimensions are $4 \times 4 \times 4$ mm^3, were employed. To evaluate the crystallinity, high-resolution XRD (a Bruker-AXS D5005 HR diffractometer, Cu-Kα radiation, HRXRD) was implemented. Double-sided polished $\langle 111 \rangle$ oriented crystal wafers with dimensions of $7 \times 7 \times 1$ mm^3 were used for the measurements.

The crystal density was characterized using the Archimedes method at room temperature. Distilled water was poured into an empty beaker. The crystal attached to hair silk was immersed in the water without touching the wall or bottom of the beaker. The density was calculated using the following formula:

$$\rho_{exp} = \frac{m_0 \cdot \rho_{water}}{m_1 - m_2}, \qquad (2)$$

where m_0 and ρ_{water} are the crystal weight in air and density of the distilled water, respectively. m_1 is the weight of the tested specimen fully immersed in the distilled water. m_2 is the weight of the distilled water and beaker. Repeated experiments were carried out to reduce the experimental error.

The transmission spectra were measured using an Agilent Cary 7000 spectrophotometer in the 200–2000 nm range. Well-polished crystal wafers with a thickness of 1 mm were used to perform the measurements.

The concentrations of elemental Al were measured by X-ray fluorescence (XRF) analysis (Rigaku, ZSX primus II). Then the effective segregation coefficients were calculated. In addition, the element content and uniformity of the as-grown TAGG75 crystals were also analysed through energy dispersive spectroscopy (EDS) using an Ultim MAX 170 (Oxford instrument).

Thermal expansion behaviors were measured in a temperature range from 25 °C to 500 °C by using a thermal expansion analyzer (Elmer, Perkin). Crystal cubes with sizes of $4 \times 4 \times 4$ mm^3 were polished on the faces for tests. Specific heat was characterized by using a differential scanning calorimeter (DSC) using a simultaneous thermal analyzer (PerkinElmer Diamond DSC) in the temperature range from 25 °C to 300 °C. Samples with dimensions of $4 \times 4 \times 1$ mm^3 were prepared for this measurement. The thermal diffusion coefficients

2424 | *J. Mater. Chem. C*, 2024, **12**, 2423–2431

This journal is © The Royal Society of Chemistry 2024

were measured by a laser pulse method using a thermal constant measuring instrument (Netzsch, LFA457) in a temperature range from 50 °C to 450 °C. The prepared crystal samples with the dimensions of $4 \times 4 \times 1$ mm^3 were coated with Au and graphite on opposite faces. The crystallographic direction of the above samples is $\langle 111 \rangle$ orientation.

The Verdet constants at wavelengths of 515, 650, and 1064 nm were measured by the extinction method. Rectangular bars with dimensions of $2.4 \times 2.4 \times 10$ mm^3 were polished on the faces perpendicular to the length direction (along [111] axis) for measurements. Ultraviolet-visible diffuse reflectance spectra (UV-vis DRS) were measured by using a Shimadzu UV-2600 spectrophotometer to explore the optical absorption. Single-crystal power was used to perform the measurements. The magnetic susceptibility was studied on a $\langle 111 \rangle$ orientation crystal plate using a physical property measurement system (PPMS Dynacool-9, Quantum Design). The magnetic field direction is parallel to the $\langle 111 \rangle$ orientation.

Results and discussion

Crystal growth

TAGG crystals were grown by the Cz method. Fig. 1 shows photographs of as-grown crystals as well as polished crystal cubes. As can be seen, a bulk single crystal with the Al substitution of up to 75% was successfully obtained, which is the highest reached Al content in TAGG reported so far. These crystals are free of cracks and inclusions. The corresponding polished cubes are illustrated in Fig. 1(f), indicating the high transparency of grown TAGG crystals. In addition, erosion streaks were observed on the crystal surface, which were caused by the re-melting during the crystal growth process. Unfortunately, only a small piece of the "polycrystal" was obtained when we grew TAGG90, indicating that the congruent composition of Al content in TAGG is less than 90%.

Fig. 2 shows the powder XRD patterns of the TAGG crystals. It can be seen that all diffraction peaks ($x \leq 0.75$) match well with the garnet structure, confirming the pure phase of the obtained crystals. In addition, the inset picture of Fig. 2(a) shows a gradual right shift of the (420) peak with the increase of

the Al content, proving the successful substitution of Al in the grown crystals since the radius of Al^{3+} (0.535 Å) is smaller than that of Ga^{3+} (0.620 Å). In the case of TAGG90, most of the XRD peaks were in good agreement with the standard card of TbAlO$_3$ (TAP, JCPDS: 20-1242). The extra peaks are consistent with TAG (JCPDS: 17-0735) as shown in Fig. 2(b). Therefore, TAGG90 is a mixed phase composed of TAP and TAG, which inherits the incongruent melting nature of TAG. Although the TAGG90 composition could possess excellent magneto-optical properties, in theory, unfavorable growth characteristics hinder its further applications.

Crystal quality

Laue back-reflection and HRXRD measurements have been widely carried out to assess the crystalline perfection and homogeneity of single crystals. As presented in Fig. 3(a), the Laue back-reflection patterns of TAGG crystals along the $\langle 111 \rangle$ orientation are clear and bright, exhibiting threefold symmetry. In Fig. 3(b), the full width at half-maximum (FWHM) values of the rocking curves of the TAGG crystals were measured to be 36.5″, 43.2″, 40.8″, and 50.3″, respectively. All of the above results confirm that the as-grown crystals are of high quality.

Density

As shown in Table 1, the average experimental densities of TAGG crystals were determined to be 7.17, 6.80, 6.46, and 6.31 g cm^{-3}, respectively, using the Archimedes method. In addition, based on the powder XRD data, the cell parameters of the TAGG crystals calculated by the software FullProf are 12.35, 12.25, 12.16, and 12.13 Å, respectively. Both the densities and lattice constants decrease linearly with the increase of the Al content.

For comparison, the theoretical density was also calculated by the following equation:

$$\rho_{\text{cal}} = \frac{M \cdot Z}{a \cdot b \cdot c \cdot N_A},\tag{3}$$

where M, Z, and N_A are the relative molecular mass, number of molecules in the unit cell, and the Avogadro constant,
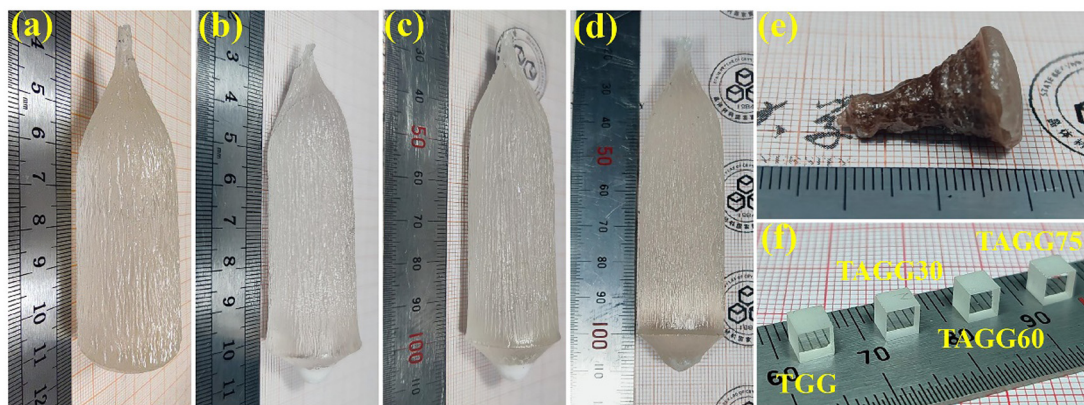

Fig. 1 Photographs of as-grown TAGG single crystals: (a) TGG, (b) TAGG30, (c) TAGG60, (d) TAGG75, and (e) TAGG90. (f) Polished crystal cubes.
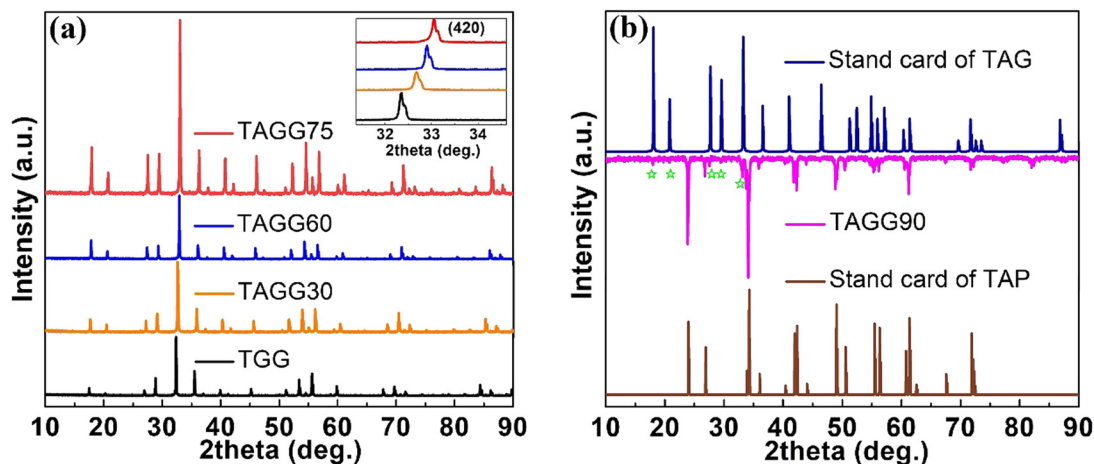
Fig. 2 (a) Powder XRD patterns of TAGG ($x \leq 0.75$) crystals. The inset shows the right shift of the enlarged (420) diffraction peaks. (b) XRD patterns of TAGG90 as well as TAG and TAP for comparison.
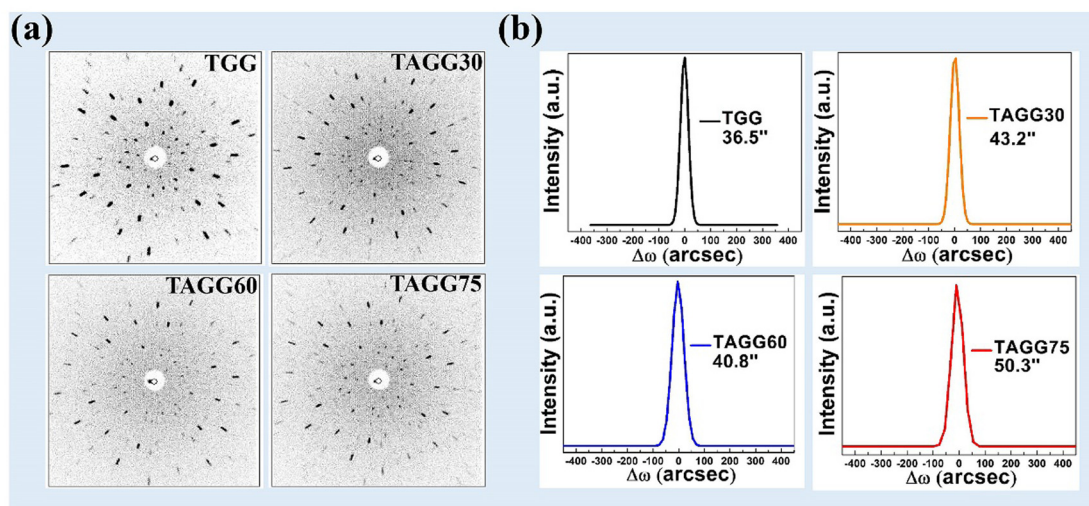

Fig. 3 Crystalline quality of as-grown TAGG crystals: (a) Laue back-reflection patterns. (b) Rocking curves.

Table 1 Average experimental densities and lattice constants of TAGG crystals

Crystal	Density (g cm^{-3})	Lattice constant (Å)
TGG	7.17	12.35
TAGG30	6.80	12.25
TAGG60	6.46	12.16
TAGG75	6.31	12.13

respectively. a, b, and c are the lattice constants. The calculated theoretical densities of TAGG crystals are 7.18, 6.90, 6.57, and 6.38 g cm^{-3}, respectively, which are very close to the measured densities. Furthermore, the Tb^{3+} concentration ($N_{Tb}{}^{3+}$) can be calculated by using the obtained lattice parameters by the following equation:

$$N_{Tb} = \frac{Z}{V}, \tag{4}$$

where Z represents the number of Tb^{3+} within a unit cell, and V denotes the volume of the unit cell. The calculated Tb^{3+} concentrations of TAGG crystals are 1.27×10^{22}, 1.31×10^{22}, 1.33×10^{22}, and 1.34×10^{22} cm^{-3}, respectively.

Transmittance

Fig. 4 shows the optical transmittance of TAGG crystals. As can be seen, as-grown TAGG ($x \leq 0.75$) crystals exhibit high transmittance of over 80% covering a wide spectral range from 400 to 1600 nm. The UV cut-off edge is located at around 290 nm, while the infrared absorption edge is about 1800 nm. More importantly, the optical transmission is gradually enhanced with the increase of the Al content. In addition, there is an obvious absorption peak centered at about 488 nm, which originates from the $^7F_6 \rightarrow {}^5D_4$ transition of the Tb^{3+}.[17] There are also several absorption peaks centered at about 353, 372, and 378 nm in the range of 300–400 nm, corresponding to the transitions $^7F_6 \rightarrow {}^5L_9$, $^5L_{10}$, and $^5G_6$ of Tb^{3+}, respectively.[18]
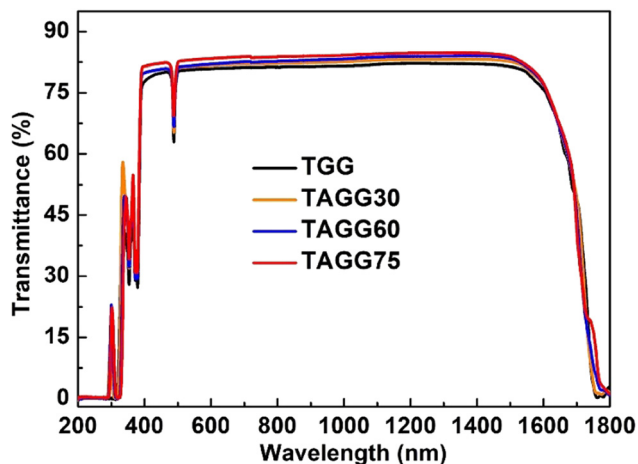
Fig. 4 Transmittance of TAGG crystals.

Chemical analysis

The chemical composition of TAGG crystals was measured by XRF measurements. The detailed information is summarized in Table 2. The effective segregation coefficients k_{eff} of Al^{3+} were calculated by the equation: $k_{\text{eff}} = C_s/C_l$, where C_s and C_l are the concentrations of the ions in the crystal and raw materials, respectively. The effective segregation coefficients k_{eff} of Al^{3+} in the TAGG30, TAGG60, and TAGG75 crystals were 1.03, 1.02, and 1.01, respectively, very close to 1, which is beneficial to large-sized and uniform crystal growth.

The composition and uniformity of the TAGG75 crystal was further determined by EDS, as given in the ESI.† Table S1 (ESI†) shows the EDS results of the TAGG75 crystal. As can be seen, the composition through EDS measurements is almost consistent with the theoretical results. In addition, the elemental mapping of Tb, Al, Ga and O is illustrated in Fig. S1 (ESI†). The elemental distribution is quite uniform in the as-grown TAGG75 crystal.

Thermal properties

The thermal properties, including thermal expansion, specific heat, thermal diffusivity, and thermal conductivity are key parameters to evaluate the potential of magneto-optical materials. Temperature-dependence of the thermal expansion for the TAGG crystals in the temperature range from 25 to 500 °C is plotted in Fig. 5(a). The garnet crystals exhibit positive thermal expansion. The linear thermal expansion coefficients α are fitted to be 8.48×10^{-6}, 8.21×10^{-6}, 7.95×10^{-6} and 7.8×10^{-6} K^{-1} for TAGG crystals, respectively. It can be seen that the

thermal expansion coefficients decrease with the increase of the Al content. The possible reason is that, compared to the Ga–O bond, the length of the Al–O bond is shorter, leading to a stronger bond strength and a more stable crystal structure.[19] Thus, the crystals are not prone to deformation under heating, resulting in a smaller thermal expansion coefficient. Fig. 5(b) shows the specific heat of TAGG crystals as a function of temperature. The specific heat of TAGG crystals at 25 °C is 0.34, 0.38, 0.40, and 0.42 J g^{-1} K^{-1}, respectively. It increases with temperature, reaching 0.44, 0.53, 0.56, and 0.60 J g^{-1} K^{-1} at 300 °C, respectively. In addition, according to the Kepp law,[20] the increasing trend of specific heat with Al content is caused by the decrease of the molar mass. The relatively large specific heat value implies that the high Al content crystals could possess better thermal stability, which is beneficial to high-power applications. Fig. 5(c) shows the measured thermal diffusivity in the temperature range from 50 to 450 °C. The thermal diffusivity decreases with rising temperature. In addition, TAGG75 shows the highest thermal diffusivity among all crystals, with a value of 1.54 mm^2 s^{-1} at 50 °C, larger than that of 1.41 mm^2 s^{-1} for the TGG crystal. However, the measured diffusivity of TGG is larger than that of TAGG30. There are two possible reasons. Firstly, for garnet crystals, the core stress could be easily formed in the center of the as-grown crystal because of the growth habits. The crystal quality in the non-stress region is better than that in the stress area. The measured samples selected from the stress zone will show poor thermal diffusion. Secondly, the difference in thermal diffusion between the TAGG samples is rather small.

Single crystals with high thermal conductivity has high heat dissipation efficiency, which is a very important parameter for magneto-optical materials, especially during high-power operation.[21] The thermal conductivity of TAGG crystals was calculated based on the following equation:

$$\kappa = \lambda \cdot \rho \cdot C_p, \tag{5}$$

where λ, ρ, and C_p are the thermal diffusivity, crystal density, and specific heat, respectively. Fig. 5(d) shows the calculated thermal conductivity of the TAGG crystals *versus* temperature. The thermal conductivity of TAGG crystals at 50 °C is 3.72, 3.42, 3.82, and 4.23 W m^{-1} K^{-1}, respectively. For nonmetallic materials, thermal conductivity is equal to the lattice thermal conductivity resulting from the phonon collision. Due to the incorporation of Al^{3+}, the interatomic bond strength becomes stronger, and the anharmonic effect of the lattice vibration becomes weaker, which will cause a low phonon collision probability.[19,22] Therefore, the thermal conductivity κ increases with increasing Al content.

Magneto-optical properties

The Faraday effect involves the rotation of plane-polarized light as it passes through a magneto-optical medium in the presence of an external magnetic field oriented parallel to the direction of light propagation, which is described by the following equation:

$$\theta = V \cdot B \cdot L, \tag{6}$$

Table 2 Chemical analysis results of TAGG crystals

Crystal	Element		
	Tb (wt%)	Al (wt%)	Ga (wt%)
TGG	57.9	0	42.1
TAGG30	63.7	5.4	31.0
TAGG60	70.6	11.2	18.2
TAGG75	74.1	14.2	11.7

This journal is © The Royal Society of Chemistry 2024

J. Mater. Chem. C, 2024, **12**, 2423–2431 | **2427**
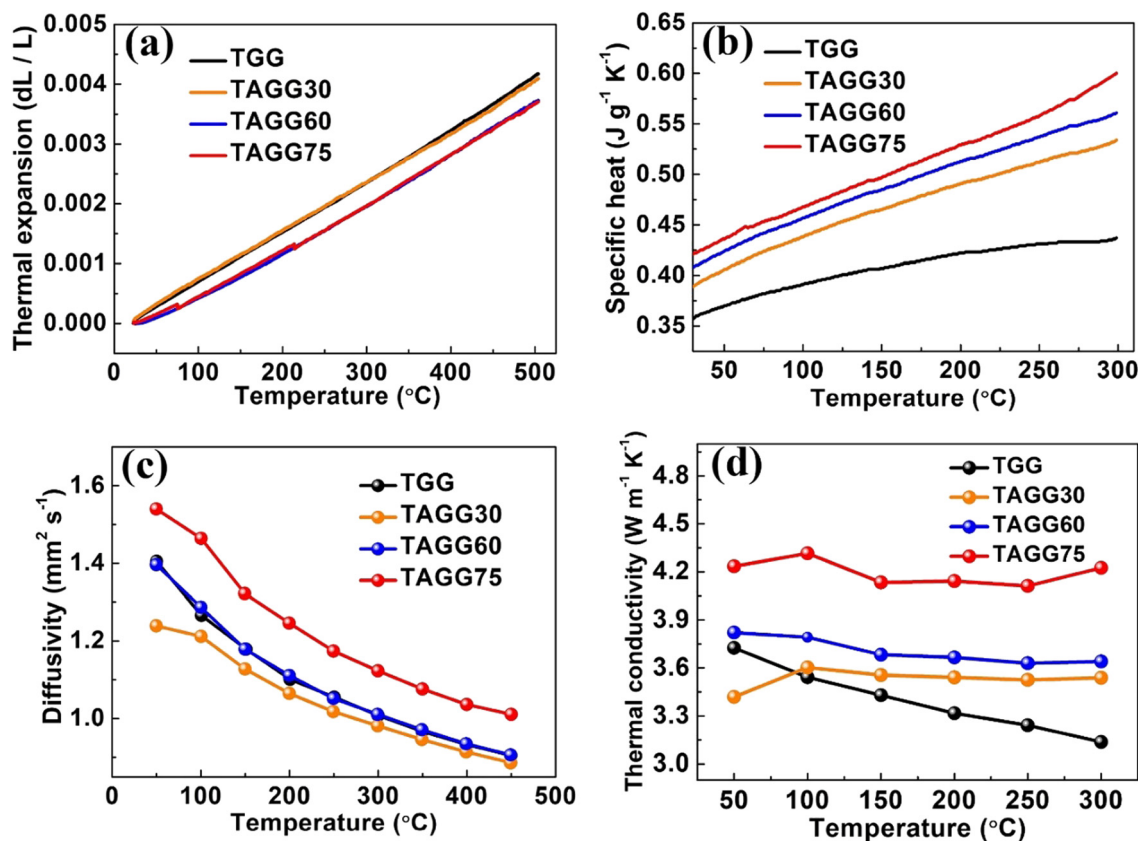
Fig. 5 Temperature-dependent thermal properties of TAGG crystals: (a) thermal expansion, (b) specific heat, (c) thermal diffusivity, and (d) thermal conductivity.

where the magnitude of the rotation θ of plane-polarized light is proportional to the strength of the applied magnetic field B, the path length L, and the wavelength-dependent Verdet constant V.

For magneto-optical materials, obtaining a large rotation angle is of prime significance to practical applications. According to eqn (6), V is the most vital parameter to characterize the capability of rotating the plane-polarized light. Magneto-optical crystals with a high V possess a better Faraday ability.

Fig. 6(a) shows the Verdet constant V of TAGG crystals at the wavelengths of 515, 650, and 1064 nm. The V value is enhanced with the increase of the Al content. The TAGG75 crystal exhibits the highest Verdet constant among these crystals. As shown in Table 3, compared with other benchmark magneto-optical crystals such as TGG,[8] TAG,[12] TSAG[23] and CeF₃,[24] the Verdet constant of TAGG crystal is comparable to that of TAG at high Al content. In addition, the experimental data were fitted as a function of V and incidence wavelength λ, given as a simplified model of Van Vleck and Hebb:[25]

$$V = \frac{E}{\lambda^2 - \lambda_0^2}, \quad (7)$$

where E is the constant term, and λ_0 is the effective transition wavelength. The corresponding fitting formulae of the TAGG crystals are $V = 4.33 \times 10^7/(\lambda^2 - 272^2)$, $V = 4.30 \times 10^7/(\lambda^2 - 312^2)$,

$V = 5.01 \times 10^7/(\lambda^2 - 301^2)$, and $V = 5.30 \times 10^7/(\lambda^2 - 285^2)$, respectively.

For Tb³⁺-based paramagnetic magneto-optical crystals, the Faraday effect originates from the $4f^8$–$4f^7 5d^1$ transition of Tb³⁺. Fig. 6(b) shows the diffuse reflection spectra of the as-grown crystals. As can be seen, there are two strong absorption peaks located at 231.4 and 263.8 nm for the TGG crystal, which derives from the $^7F_6$ ($4f^8$) → ^7E ($4f^7 5d^1$), $^7T_2$ ($4f^7 5d^1$) and $^7F_6$ ($4f^8$) → ^9E ($4f^7 5d^1$), $^9T_2$ ($4f^7 5d^1$) transitions, respectively. In addition, the absorption peaks are red-shifted with the increase of the Al content, indicating that the Tb³⁺ in the TAGG crystal is under a stronger crystal field environment (the decrease of lattice constant leads to the stronger crystal field), which results in a higher energy level splitting.

The moment of TAGG crystals in the range of −2 T to 2 T is presented in Fig. 6(c). The moment increases with the increase of the magnetic field, which can be expressed by the following equation:

$$M = \chi \cdot H, \quad (8)$$

where M is the moment, χ is the magnetic susceptibility, and H is the applied magnetic field. The slope of the curve represents the magnetic susceptibility of the crystal. The χ values of the TAGG crystals are 1.14, 1.22, 1.29, and 1.35 emu g⁻¹ T⁻¹, respectively. This proves that the TAGG crystal with higher Al
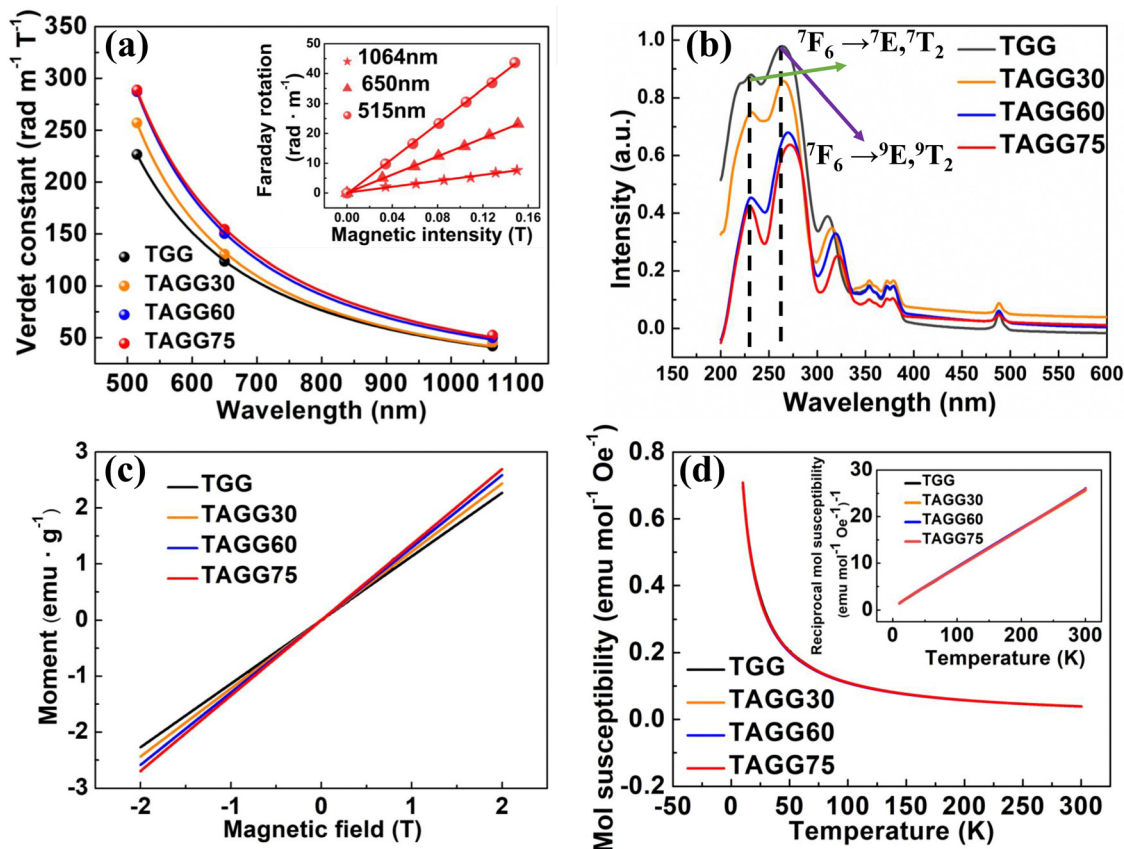
Fig. 6 (a) Verdet constant of TAGG crystals at the wavelengths of 532, 650, and 1064 nm. The inset shows the Faraday rotation angles of the TAGG75 crystal as a function of magnetic intensity and wavelength. (b) Diffuse reflection spectra of TAGG crystals. (c) The moment in the range of −2 T to 2 T at room temperature. (d) Temperature dependence of the mol susceptibility. The inset shows the reciprocal mol susceptibility *versus* temperature ($H = 2$ T).

Table 3 Verdet constants of TAGG and other benchmark magneto-optical crystals at a wavelength of 1064 nm

Crystals	V@1064 nm (rad m^{-1} T^{-1})	Ref.
TGG	−40	8
TAG	−52	12
TSAG	−47.8	23
CeF$_3$	−35.7	24
TGG	−41.8	This work
TAGG30	−45.4	
TAGG60	−49.9	
TAGG75	−52.4	

content can be more easily magnetized at the same magnetic field, further leading to the superior Faraday effect.[26]

In order to study the temperature-dependence of the magneto-optical properties of the above crystals, the mol susceptibility χ_{mol} in the temperature range of 10–300 K at a certain external magnetic field ($H = 2$ T) was measured, as shown in Fig. 6(d). It can be seen that the TAGG crystals exhibit paramagnetic behavior. With the increase in temperature, the mol susceptibility decreases. At the same time, the rate of decrease gradually becomes lower.

The inset picture of Fig. 6(d) shows the reciprocal mol susceptibility *versus* temperature ($H = 2$ T). The linear part of the $\chi^{-1}(T)$ curve can be described by the Curie—Weiss

equation:[27]

$$\chi = \frac{C}{T - \theta_{cw}} \quad (9)$$

where C is known as the Curie constant, T is the temperature, and θ_{cw} is often referred to as the Curie–Weiss temperature. The fitted data give the θ_{cw} values as −10.11, −10.20, −9.11, and −8.25 K for TAGG crystals, respectively. The negative Curie–Weiss temperature indicates the dominance of the antiferromagnetic interactions between Tb^{3+} ions.[28] In addition, the Curie constant of TAGG crystals is fitted to be 12.07, 12.08, 11.95, and 11.97, respectively. The Curie constant is related to the number of unpaired electrons, which can be used to calculate the effective magnetic moment (μ_{eff}) per ion (Tb^{3+}) in units of Bohr magnetons (μ_B) using equation $\mu_B = \sqrt{8C}\mu_B$. The effective magnetic moments of TAGG crystals are 9.83, 9.83, 9.78, and 9.78μ_B, respectively, consistent with reported data.[27] According to the quantum theory of the magneto-optical effect of the paramagnetic materials,[11,25,26] the verdet constant V can be described by the following equation:

$$V = \left(\frac{A}{T}\right)\left(\frac{Nn_{eff}^2}{g}\right)\left\{\frac{C_i}{1 - (\lambda/\lambda_i)^2}\right\}, \quad (10)$$

This journal is © The Royal Society of Chemistry 2024

J. Mater. Chem. C, 2024, **12**, 2423–2431 | **2429**

Where A is the wavelength-independent constant, T is the temperature, N is the paramagnetic ion number per unit volume, n_{eff} is determined by the effective magnetic quantum number, g is the Lande splitting coefficient, λ_i is the effective transition wavelength, and C_i is the effective transition probability. For Tb^{3+}-based paramagnetic magneto-optical crystals, the Verdet constant is mainly derived from concentration N, $4f^8 \rightarrow 4f^7 5d^1$ effective transition wavelength, and the effective transition probability of Tb^{3+}.[11] In the case of TAGG crystals, when the Al content increases, the Tb^{3+} ion number per unit volume increases with the decrease of the cell volume because the radius of Al^{3+} is smaller than that of Ga^{3+}, further leading to the shorter bond length of $Tb^{3+}-O^{2-}$ in the TAGG crystal. The higher the Al content in TAGG, the shorter the bond length of $Tb^{3+}-O^{2-}$, Tb^{3+} in the TAG crystal is in a stronger crystal field environment that results in a greater energy level splitting of Tb^{3+}, the effective transition probability is improved, and the effective transition wavelengths $^7F_6 \rightarrow {}^7E, {}^7T_2$, and $^7F_6 \rightarrow {}^9E, {}^9T_2$ are also red-shifted.

The Verdet constant is directly proportional to the magnetic susceptibility χ as follows:

$$V = \left(\frac{4\pi^2\nu^2\chi}{g\mu_B ch}\right) \sum_{ij} \frac{C_{ij}}{\nu^2 - \nu_{ij}^2}, \qquad (11)$$

where ν is the frequency of the incident light, ν_{ij} is the transition frequency between electronic states, C_{ij} is the transition probability, g is the Landé factor, μ_B is the Bohr magneton, c is the velocity of light, and h is the Planck constant. According to eqn (11), when the magnetic susceptibility χ increases, V increases. In summary, all the above factors include the paramagnetic ion number per unit volume, effective transition wavelength, effective transition probability, and magnetic susceptibility, contributing to the improvement of the Verdet constant.

Conclusions

In summary, TAGG crystals with different Al contents were grown by the Cz method. High-quality single crystals with even a record of 75% Al-substitution were successfully achieved for the first time. Only a small piece of the "polycrystal" was obtained in the case of TAGG90. The high crystalline quality of the grown crystals ($x \leq 0.75$) was confirmed by Laue and HRXRD measurements. The effective segregation coefficient of Al is very close to 1, which is beneficial to large-sized and uniform crystal growth. Then, the effect of Al substitution on the properties of the TAGG crystals ($x \leq 0.75$) was systematically investigated. With the increase of the Al content, the transmittance improved, and the thermal properties of specific heat, thermal diffusivity, and thermal conductivity were enhanced; more importantly, the Verdet constant elevated 25–30%. The TAGG crystal with 75% Al substitution exhibits the best performance, that is, the highest transmittance of over 80%, the largest thermal conductivity of 4.23 W m^{-1} K^{-1} at 50 °C, and the highest Verdet constants of 288.6, 154.3 and 52.4 rad m^{-1} T^{-1} at wavelengths of 515, 650 and 1064 nm, respectively. Therefore, the TAGG75 single crystal is very promising for Faraday isolators.

Conflicts of interest

There are no conflicts to declare.

Acknowledgements

References

1 K. J. Carothers, R. A. Norwood and J. Pyun, High Verdet Constant Materials for Magneto-Optical Faraday Rotation: A Review, *Chem. Mater.*, 2022, **34**(6), 2531–2544.

2 O. V. Palashov, D. S. Zheleznov, A. V. Voitovich, V. V. Zelenogorsky, E. E. Kamenetsky, E. A. Khazanov, R. M. Martin, K. L. Dooley, L. Williams and A. Lucianetti, High-vacuum-compatible high-power Faraday isolators for gravitational-wave interferometers, *J. Opt. Soc. Am. B*, 2012, **29**(7), 1784–1792.

3 B. J. Stadler and T. Mizumoto, Integrated magneto-optical materials and isolators: a review. A Review, *IEEE Photonics J.*, 2013, **6**(1), 1–15.

4 S. J. Czuchlewski, A. V. Nowak, E. Foley and J. F. Figueira, Broad-band gas isolator for high-power CO$_2$-Lasers, *Opt. Lett.*, 1978, **2**(2), 39–41.

5 Y. Hao, X. Xin, X. Yang, Z. Zhang, X. Fu, Z. Jia and X. Tao, Reporting a novel visible near-infrared {Tb3}[Ga0.1Sc1.9](Al3)O12 single crystal for Faraday isolators, *J. Mater. Chem. C*, 2023, **11**(28), 9727–9734.

6 R. Dou, H. Zhang, Q. Zhang, N. Zhuang, W. Liu, Y. He, Y. Chen, M. Cheng, J. Luo and D. Sun, Growth and properties of TSAG and TSLAG magneto-optical crystals with large size, *Opt. Mater.*, 2019, **96**, 109272.

7 K. Shimamura, T. Kito, E. Castel, A. Latynina, P. Molina, E. G. Víllora, P. Mythili, P. Veber, J.-P. Chaminade and A. Funaki, Growth of {Tb$_3$}[Sc$_{2-x}$Lu$_x$](Al$_3$)O$_{12}$ Single Crystals for Visible-Infrared Optical Isolators, *Cryst. Growth Des.*, 2010, **10**(8), 3466–3470.

8 Z. Chen, L. Yang, Y. Hang and X. Wang, Faraday effect improvement by Dy3+-doping of terbium gallium garnet single crystal, *J. Solid State Chem.*, 2016, **233**, 277–281.

2430 | *J. Mater. Chem. C*, 2024, **12**, 2423–2431

This journal is © The Royal Society of Chemistry 2024

9 Z. Chen, L. Yang, X. Wang and H. Yin, High magneto-optical characteristics of Holmium-doped terbium gallium garnet crystal, *Opt. Lett.*, 2016, **41**(11), 2580–2583.

10 X. Wang, L. Yang, Z. Chen, J. Wang, J. Hong, Y. Wang, C. Shi, P. Zhang, L. Zhang and Y. Hang, Growth and Faraday rotation characteristics of $Tb_{3-x}Nd_xGa_5O_{12}$ single crystal, *Opt. Mater.*, 2015, **47**, 157–160.

11 H. Liu, G. Zhan, G. Wu, C. Song, X. Wu, Q. Xu, X. Chen, X. Hu, N. Zhuang and J. Chen, Improved Edge-Defined Film-Fed Growth of Incongruent-Melting $Tb_3Al_5O_{12}$ Crystal with High Magneto-Optical and Thermal Performances, *Cryst. Growth Des.*, 2019, **19**(3), 1525–1531.

12 M. Geho, T. Sekijima and T. Fujii, Growth mechanism of incongruently melting terbium aluminum garnet ($Tb_3Al_5O_{12}$: TAG) single crystals by laser FZ method, *J. Cryst. Grow.*, 2005, **275**(1–2), e663–e667.

13 L. Li, Y. Yu, S. Zhang, T. Chen, T. Zheng and L. Hang, Eliminate of cracking for the growth of large-size $Tb_3Sc_2Al_3O_{12}$ crystals, *J. Cryst. Grow.*, 2022, **579**, 126458.

14 D. A. Pawlak, Y. Kagamitani, A. Yoshikawa, K. Wozniak, H. Sato, H. Machida and T. Fukuda, Growth of Tb–Sc–Al garnet single crystals by the micro-pulling down method, *J. Cryst. Grow.*, 2001, **226**(2), 341–347.

15 X. Xin, Y. Hao, L. Liu, J. Lv, J. Zhang, X. Fu, Z. Jia and X. Tao, $Tb_3Al_3Ga_2O_{12}$: A Novel Visible–Infrared Faraday Crystal Exhibiting a Superior Magneto-Optical Performance, *Cryst. Growth Des.*, 2022, **22**(9), 5535–5541.

16 W. Zhang, F. Guo and J. Chen, Growth and characterization of $Tb_3Ga_{5-x}Al_xO_{12}$ single crystal, *J. Cryst. Grow.*, 2007, **306**(1), 195–199.

17 W. Z. Jin, J. X. Ding, L. Guo, Q. Gu, C. Li, L. B. Su, A. H. Wu and F. M. Zeng, Growth and performance research of $Tb_3Ga_5O_{12}$ magneto-optical crystal, *J. Cryst. Grow.*, 2018, **484**, 17–20.

18 D. Vijayasri, K. S. Rudramamba, T. Srikanth, N. M. Reddy, M. Nakka, S. Pratyusha and M. R. Reddy, Spectroscopic features of Tb3+ doped strontium zinc borate glasses for green laser applications, *J. Mol. Struct.*, 2023, 1274.

19 J. Zhang, Z. Zhang, Y. Sun, C. Zhang and X. Tao, Anisotropic thermal properties of the polar crystal $Cs_2TeMo_3O_{12}$, *J. Solid State Chem.*, 2012, **195**, 120–124.

20 Z. D. Guan, Z. T. Zhang and J. S. Jiao, *Phys. Prop. Inorg. Mater.*, 1992, 327.

21 J. Xu, H. Wu, H. Yu, W. Zhang, Z. Hu, J. Wang, Y. Wu and P. S. Halasyamani, $Li_2K_4TiOGe_4O_{12}$: A stable mid-infrared nonlinear optical material, *Chem. Mater.*, 2019, **32**(2), 906–912.

22 J. D. Patterson and B. C. Bailey, *Solid-state physics: introduction to the theory*. Springer Science & Business Media, 2007.

23 L. Li, T. Chen, Y. Yu, S. Zhang and Z. Yu, Study on the Solid and Solution Properties of Sc3+ and Al3+ in (Tb, Sc)3(Sc, Al)-5O12 Crystals Grown by the Czochralski Method, *Cryst. Growth Des.*, 2023, **23**(8), 5950–5956.

24 G. Zhao, C. Zhao, Y. Yang, M. Xu, S. Li and Y. Hang, Magneto-optical performances of novel neodymium-doped CeF_3 crystal, *Mater. Lett.*, 2021, 300.

25 Z. Chen, Y. Hang, X. Wang and J. Hong, Fabrication and characterization of TGG crystals containing paramagnetic rare-earth ions, *Solid State Commun.*, 2016, **241**, 38–42.

26 Y. Kagamitani, D. A. Pawlak, H. Sato, A. Yoshikawa, J. Martinek, H. Machida and T. Fukuda, Dependence of Faraday effect on the orientation of terbium–scandium–aluminum garnet single crystal, *J. Mater. Res.*, 2011, **19**(2), 579–583.

27 S. Mugiraneza and A. M. Hallas, Tutorial: a beginner's guide to interpreting magnetic susceptibility data with the Curie-Weiss law, *Commun. Phys.*, 2022, **5**, 1.

28 P. Man, F. Ma, T. Xie, J. Ding, A. Wu, L. Su, H. Li and G. Ren, Magneto-optical property of terbium-lutetium-aluminum garnet crystals, *Opt. Mater.*, 2017, **66**, 207–210.

This journal is © The Royal Society of Chemistry 2024

J. Mater. Chem. C, 2024, **12**, 2423–2431 | **2431**